Isomorphous PrT_2B_2C (T=Co,Ni,Pt) single crystals: Structural, transport, and magnetic properties

A. Durán,[1] S. Bernès,[2] R. Falconi,[3] R. Escudero,[4] O. Laborde,[5,*] and M. Guillot[5]
[1]*Centro de Ciencias de la Materia Condensada, Universidad Nacional Autónoma de México, AP 2681, Ensenada 22800, B. C., Mexico*
[2]*Facultad de Ciencias Químicas, Universidad Autónoma de Nuevo León, 64570 Monterrey N.L., Mexico*
[3]*División Académica de Ciencias Básicas, Universidad Juárez Autónoma de Tabasco, Cunduacán, Tabasco 86690, AP 24, Mexico*
[4]*Instituto de Investigaciones en Materiales, Universidad Nacional Autónoma de México, AP 70-360, México D. F., 04510, Mexico*
[5]*Centre des Recherches Sur les Très Basses Temperatures, CNRS, BP 166, 38042 Grenoble Cedex 09, France*
(Received 13 September 2005; revised manuscript received 1 May 2006; published 27 October 2006)

The full substitution of Ni by Co and Pt enclosed in the same crystalline structure ($I4/mmm$) of Pr-based compounds have been investigated. The structural characteristics, magnetic properties, and magnetoresistance of $PrCo_2B_2C$, $PrNi_2B_2C$, and $PrPt_2B_2C$ single crystals were studied to determine the reason for the absence or presence of superconductivity in those compounds. An antiferromagnetic transition was found for $PrCo_2B_2C$ at about 8.5 K, where the easy magnetization axis is along the c-crystallographic direction whereas in $PrNi_2B_2C$ the easy magnetization was at the ab plane. In $PrNi_2B_2C$ a small magnetization without traces of saturation is found when it is measured up to 18 Tesla of applied magnetic field. This behavior suggests a screening effect as a result of a moderate hybridization between the conduction band and Pr ions. Superconductivity occurs in $PrPt_2B_2C$ at about 6 K. The Pt-Pt distance and internal bonding angles are similar to those observed in the superconducting Ni-based compounds. Magnetoresistance measurements show positive and quadratic behavior ($\Delta\rho/\rho_0 \sim aH^2$) suggesting a spin fluctuation system. In the $PrPt_2B_2C$ compound the electronic mean free path is smaller than the BCS coherence length ($\iota \ll \varepsilon$) suggesting a dirty type II superconductor.

DOI: 10.1103/PhysRevB.74.134513 PACS number(s): 74.25.Bt, 74.25.Ha

I. INTRODUCTION

Quaternary borocarbides form a family of intermetallic compounds with a wide variety of collective phenomena at low temperatures that have generated a great deal of experimental and theoretical work.[1,2] The general $LuNi_2B_2C$-type structure permits the incorporation of rare earth elements (except Eu), and transition metals such as Ni, Ir, Pt, Co, Pd, and Ru.[1–4] An interesting aspect of these materials is that they are prototypical systems suitable for the study of the coexistence and/or competition between magnetism and superconductivity.[5–7] Both phenomena are related to different types of interactions; Ruderman, Kittel, Kasuya, Yosida (RKKY), crystalline electric field (CEF) effects, and electron-phonon coupling. The main effects come from the RKKY interaction and CEF due to the coupling between f-electrons and d-electron band, responsible for a wide variety of magnetic phenomena.[1,5–7]

Experimental studies in these compounds show that the de-Gennes factor roughly decreases with the superconducting transition temperature (T_c), indicating a weak magnetic interaction between rare earth ions and conduction electrons. These results could imply that the superconductivity is expected not only for the heavy rare earth ions, but also for the light ones.[8] Band structure calculations for $LuNi_2B_2C$ and YNi_2B_2C (Lu, Y/Ni221) superconductors show a peak at the Fermi level with a large contribution to the density of states (DOS) from the $3d$ nickel band, whereas in light rare earth compounds, the DOS is drastically reduced showing a valley at the Fermi level, a fact that accounts for the absence of superconductivity in these compounds.[1,9,10] On the other hand, the complete substitution of Ni by Pt in La and Pr borocarbides leads to superconductivity at 10 and 6 K, respectively.[11] The singular electronic behavior of these compounds has attracted attention because they are the first superconducting systems with light rare earth elements in the modified $ThCr_2Si$ structure. In this family, the compounds formed with $Pr(Ni,Co)_2B_2C$ show long range magnetic ordering and superconducting behavior for the case of $PrPt_2B_2C$ compound.[11–13] It is worth mentioning that there are only a few praseodymium based compounds that present superconductivity; that is, among the high T_c ceramic superconductors, only those with partial substitutions of praseodymium in the T' phase (R_2CuO_4) have been found superconducting while in the $PrBa_2Cu_3O_{7-x}$ compound the possibility of superconductivity is still questioned and is under discussion.[14,15] However, superconductivity has been found in the following intermetallic systems; $PrMo_6(S,Se)_8$ compounds ($T_c \sim 4$, and 9 K),[16] borocarbide $PrPt_2B_2C$ ($T_c \sim 6$ K),[11] and recently in the $PrOs_4Sb_{12}$ which is a heavy fermion skutterudite with $T_c \sim 1.8$ K.[17]

Under this scenario a systematic study of the changes observed in structural and electronic properties for PrT_2B_2C (T=Ni, Co, and Pt) single crystals is presented. The exchange of Ni by Co or Pt increases the c parameter with an anomalous contraction of the ab plane. In $PrCo_2B_2C$ a strong anisotropy is observed in the magnetic properties, with the easy spin orientation in the [001] direction, instead of the [110] direction found by neutron diffraction experiments in the $PrNi_2B_2C$ compound. The complete substitution of Ni by Pt causes significant changes in the electronic properties, which lead to one of these uncommon superconducting ma-

terials ($T_c \sim 6$ K) where nonmagnetic ordering has been found down to 1 K. The electronic mean free path is smaller than the BCS coherence length leading to dirty type II superconductor ($\iota \ll \varepsilon_0$). The Ginzburg-Landau parameters are discussed and compared with homologue quasiclean Ni-superconductor systems.

II. EXPERIMENTAL DETAILS

Single crystals were grown using a water cooled copper crucible in a radio frequency induction furnace.[18] The purity of the starting materials was Pr 99.9%, Ni 99.9%, Co 99.99%, Pt 99.9%, B 99.8%, and C 99.9998%. As-grown single crystals were used for this study (degradation processes in samples annealed for long periods of time have been observed). The samples were studied by x-ray diffraction, using a Bruker P4 diffractometer at room temperature with monochromatized Mo-K_α radiation ($\lambda = 0.710\,73$ Å, 50 KV, 30 mA). Cell parameters were refined using a large set of centered reflections. A complete diffraction sphere (eight octants merged in the $I4/mmm$ space group) was measured[19] for each crystal, up to the highest resolution achievable, namely 0.50 Å for $PrCo_2B_2C$ and 0.58 Å for $PrPt_2B_2C$. Raw data were corrected for absorption effects on the basis of ψ scans, considering the crystals as laminar. The structures were refined by full matrix least squares, using atomic scattering factors provided by the program package SHELXL-97 (Ref. 20). In the last cycles, extinction effects were corrected through a semiempirical formula[21] and convenient weighting schemes were applied to the structure factors. In the case of $PrPt_2B_2C$, B and C atoms were refined isotropically, to avoid nonpositive thermal ellipsoids for these atoms. Very large residuals are observed in the final difference Fourier maps, particularly for the $PrPt_2B_2C$ refinement, which should be attributed to somewhat inaccurate absorption corrections rather than to actual residual electronic density. Complete data, including structure factors, are available on request as CIF files.

The magnetization data presented here were obtained using a quantum design SQUID magnetometer with the magnetic field applied along the *a*-*b* and *c* directions of the platelike single crystals with typical dimension of about $1.5 \times 0.5 \times 0.3$ mm. The $M(H,T)$ data were taken under zero field cooling (ZFC) and field cooling (FC) modes. Magnetization vs applied magnetic field measurements was extended up to 18 Tesla at the CNRS-Max Planck High Magnetic Fields Laboratory, at Grenoble, France.

Resistivity measurements were performed from 2–300 K using four 25 μm gold wires attached with silver paint to the crystal and the applied ac flowing in the *ab* plane. Magnetoresistance measurements were performed with a 7.8 Tesla superconducting magnet using 20 μm gold wires with an injected current of 10 mA using a standard four-probe technique. The samples were carefully aligned and fixed with glue, and the magnetic field perpendicularly applied to the *ab* plane at constant temperature.

III. RESULTS AND DISCUSSION

A. X-ray single crystal analysis of PrT_2B_2C with T=Ni, Co, and Pt

As expected, the $I4/mmm$ space group was confirmed from the intensity measurements of symmetry-related reflections for $PrCo_2B_2C$ and $PrPt_2B_2C$ crystals. In the first case, no extra spots were detected on the photographic plates, revealing the single crystal nature; in contrast, the $PrPt_2B_2C$ crystal displays some diffuse spots, suggesting a different mosaic structure. The difference is clearly seen by the lowest diffraction intensity in $PrPt_2B_2C$ compared to $Pr(Ni,Co)_2B_2C$ crystal. However, it was possible to obtain an accurate structural analysis. The atomic coordinates and the thermal parameters (U_{eq}) from the refinement cycling are included in Table I. Lattice parameters, metal-metal bond lengths and motion of the internal bonding of TB_4 framework parameters are listed in Table II, for isomorphic PrT_2B_2C [T=Ni,[22] Co, and Pt] single crystals.

TABLE I. Atomic coordinates and equivalent isotropic displacement parameters at room temperature for the PrT_2B_2C (T =Ni,Co,Pt) compounds.

Site	x	y	z	U_{eq} (Å^2)
$PrNi_2B_2C$				
Pr	0	0	0	0.00588(12)
Ni	1/2	0	1/4	0.00663(14)
C	1/2	1/2	0	0.0075(9)
B	0	0	0.3514(3)	0.0092(4)
$PrCo_2B_2C$				
Pr	0	0	0	0.00671(9)
Co	1/2	0	1/4	0.00584(10)
C	1/2	1/2	0	0.0151(9)
B	0	0	0.3506(5)	0.0140(6)
$PrPt_2B_2C$				
Pr	0	0	0	0.0065(2)
Pt	1/2	0	1/4	0.00527(18)
C	1/2	1/2	0	0.003(3)
B	0	0	0.3626(12)	0.0076(14)

The main structural characteristics observed in $PrPt_2B_2C$ when Ni is substituted by Co, or Pt can be summarized in the following manner: Co and Pt have ionic radii of 0.72 and 0.80 Å as compared to 0.69 Å for Ni, and hence one would expect a lattice expansion by complete Co or Pt substitution. However, the structural analysis shows that the Co based compound presents a cell volume slightly contracted as compared to the Ni compound. This is an inconsistent behavior from the viewpoint of a chemical-pressure effect. For the Pt-based compound, the cell volume is increased by about 14%, consistent with the larger ionic radius of this metal.

The anomalous contraction observed in $PrCo_2B_2C$ is reflected in the structural parameters, mainly at the Co-Co bond length in the *ab* planes. The Co-Co distance is the shortest observed in these three compounds. However, we noted that the Ni-Ni and Co-Co distances in $PrNi_2B_2C$ and $PrCo_2B_2C$ are both still slightly larger than the corresponding T-T distances observed in the superconducting (Y,R)Ni-based compounds.[3,18] The short Co-Co bond length gives raise to a reduction of the B-Co distance within the CoB_4 tetrahedra, which in turn, decreases the *a* parameter by about 2.2% of the unit cell. The simultaneous increase of

TABLE II. Structural parameters and selected interatomic distances obtained from the single crystal x-ray study of PrT_2B_2C with T =Ni [22], Co, and Pt. a, c, and V are the until cell parameters. T-T is the shortest distance between 3d ions in the layers at z=1/4; T-B is the bond length between 3d ions and B atoms; T_2B_2 is the thickness of the layer at z=1/4 and B-T-B is the acute angle within T_2B_2 layers.

Compound	Ionic radii (T) (Å)	a (Å)	c (Å)	V (Å^3)	T-T (Å)	T-B (Å)	T_2B_2 Layer thickness (Å)	B-T-B Tetrahedral angle (°)
$PrNi_2B_2C$	0.69	3.6996(2)	9.9885(8)	136.71(1)	2.6160(1)	2.109(2)	2.026	103.33(7)
$PrCo_2B_2C$	0.72	3.6156(1)	10.3507(6)	135.31(1)	2.5566(1)	2.086(3)	2.082	104.4(1)
$PrPt_2B_2C$	0.80	3.8373(1)	10.7610(9)	158.45(1)	2.7134(1)	2.269(7)	2.424	106.6(3)

3.4% for the c parameter yields a distortion of the tetrahedral TB_4 framework, with bond angles B-T-B of 104.4(1)° in $PrCo_2B_2C$, instead of 103.33(7)° as found for $PrNi_2B_2C$; in other words, when compared with the Co-based phase, the Ni-based phase presents a smoothing of the T_2B_2 layers normal to the c axis, which is directly related to the thickness of this layer (see Fig. 1 and Table I). On the other hand, the full isostructural substitution of Ni by Pt significantly modifies the c and a parameters, as expected from the large Pt ionic radius. In $PrPt_2B_2C$, the Pt-Pt distance of 2.7134(1) Å in the ab plane is shorter than the atomic distance expected from the metallic Pt-Pt fcc distance (2.77 Å), suggesting not only strong metal-metal bonding, but also a decrease in the stability of the RPt_2B_2C compounds with other smaller R lanthanide ions.[3] Furthermore, it is noted that the distance between the Pt_2B_2 and the Pr-C layer, $d_{B\text{-}C}$=1.478(9) Å, is quite close to the distance between the Ni_2B_2 and the Pr-C layer, $d_{B\text{-}C}$=1.484(3) Å, but slightly larger in Pr/Co compound, $d_{B\text{-}C}$=1.546(6) Å. This rigid bond has been observed without appreciable change in the whole series of R/Ni borocarbides.[3,23] In the internal TB_4 framework it is observed that the layer thickness increases about 2.76% and 19.4% when Ni is substituted by Co and Pt, respectively. This behavior suggests a significant weakness of the covalent bonds of the 5d Pt orbitals with 2p-B nearest neighbor. The increase of 7.7% in the c parameter for $PrPt_2B_2C$ respect to the Ni-based compound is reflected not only by the large B-T-B bond angle of the tetrahedral TB_4 framework, from 103.33(7) for Ni-based to 104.43(12) for Co-based compounds, to 106.6(3)° for the Pt-based (α in Fig. 1), but also by the Pt_2B_2 layer thickness, contrary to the Co-based compound, where the c parameter is influenced by a slight increase of both, B-C distance and the B-T-B bond angle.

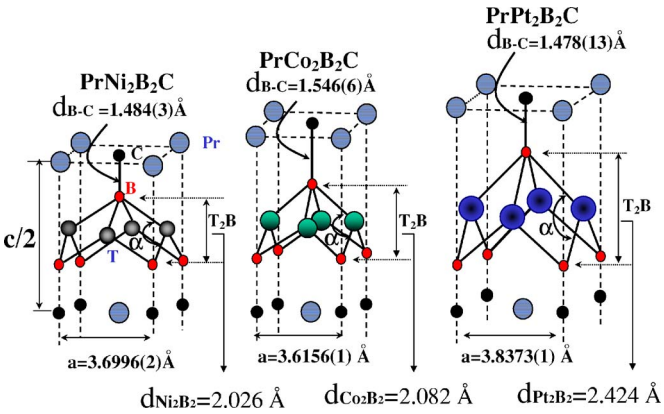

FIG. 1. (Color online) Representation of the crystal structure showing the main Pr-C layer and T_2B_2 (T=Ni, Co, and Pt) slabs in one-half (c/2) of the $LaNi_2B_2C$-type structure ($I4/mmm$ space group). Structures show the main change of the $d_{B\text{-}C}$, T_2B_2 layer thickness, and the internal angles (α) as described in the text.

From the point of view of electronic structure calculations,[9,10] the lack of superconductivity in the large lanthanide ions in the Ni-based borocarbides has been attributed to the decrease in the density of states (DOS) at the Fermi level, caused by changes in the internal structural features. From this picture, the changes in B-T-B angles observed in $PrNi_2B_2C$ and $PrCo_2B_2C$ might explain the disappearance of superconductivity via reduction of the DOS. In contrast, the structural changes in $PrPt_2B_2C$ favor the increase of the DOS at $N(E_F)$, as well as an increase of the electron-phonon coupling. This is in agreement with the fact that the structural parameters observed in the $DyNi_2B_2C$ superconductor, where the Ni-B-Ni=107.03(6)° angle and the Ni-Ni=2.5017(1) Å length are similar. In both systems superconductivity appears at about 6 K.[24,25]

Another significant feature which should be noted from the single-crystal diffraction patterns is the characteristic sharp peak profiles observed for $PrPt_2B_2C$, compared to the Pr-Ni and Pr-Co samples. A qualitative explanation may be related to a low defect concentration in the Pt-based compound.

B. Resistivity and magnetization measurements in $PrCo_2B_2C$

The temperature dependence of the susceptibility in the ZFC mode under an applied field of 100 Oe along with the resistivity measured from 50 to 2 K for a $PrCo_2B_2C$ single crystal are shown in Fig. 2. A slight resistivity drop is observed at ~20 K with a tendency to saturation below that temperature. A minimum value of about 1.7 $\mu\Omega$ cm was found at 2 K. The transition temperature is made evident as a peak at ~8.5 K of the susceptibility versus temperature plot. The continuous decrease of the resistivity and the peak in the susceptibility data are clear evidence of antiferromagnetic order (AFM). This AFM transition becomes broader and quite similar to that found in $PrNi_2B_2C$ and other rare earth compounds of this family.[22,26] The residual resistivity ratio (RRR) measured in the ab plane is about 32 which is larger than that of $PrNi_2B_2C$ single crystals[22] even to reach similar values of RRR to that produced by flux growth in RNi_2B_2C parent single crystals compounds (see Table III). A rough estimation of the electronic mean-free path l using the rela-

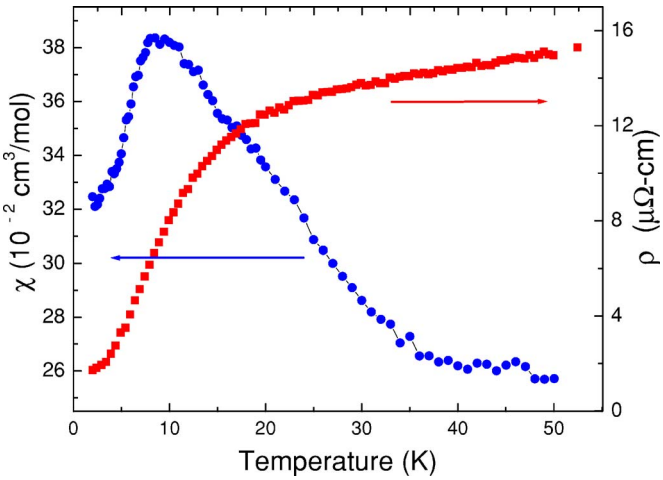

FIG. 2. (Color online) Susceptibility (filled circles) and resistivity (filled squares) measurements as functions of temperature from 50 to 2 K with an applied magnetic field of 100 Oe in the *ab* plane for a $PrCo_2B_2C$ single crystal.

tion given in Ref. 27, yields a value of 183 Å, almost twice as large as that for $PrNi_2B_2C$ (l=97 Å).

Figure 3(a) shows the temperature dependence of the susceptibility $\chi(T)$ in a 100 Oe applied magnetic field parallel to the *ab* plane and to the *c* axis for a $PrCo_2B_2C$ crystal. The inset shows an expanded plot below 30 K. In the studied temperature range, the susceptibility data does not obey Curie-Weiss law even when the temperature-independent susceptibility term, χ_0, is included. The reason for this behavior is that, at about 155 K, there is a change in the susceptibility data in both directions. The jump in the susceptibility at 155 K, in the *ab* plane is smaller (0.18 emu/mol) than in the *c* direction (0.37 emu/mol). It is important to mention that this anomaly is quite similar in shape to the jump observed in magnetization measurements at 15 K in $PrNi_2B_2C$ crystals, although the temperature is one order of magnitude higher. In that case[22] the possibility that the anomaly at 15 K could be explained under a spin canted scenario in Pr ion and/or as a ferrimagnetic transition due to the two magnetic sublattices was discussed, and this fact was related to the absence of superconductivity. At low temperature, the AFM transition takes place at about 8.5 K and it is manifested as a broad peak in the susceptibility measurements [see inset in Fig. 3(a)]. Indeed, a large magnetic anisotropy is observed when the magnetic field is applied along the *ab* plane and the *c* axis. This anisotropic behavior is similar to other RT_2B_2C (R=rare earth, and T=Ni,Co) single crystals where the strong anisotropy was attributed to CEF interactions.[7,26] A rather surprising result of this work is that the total substitution of Ni by Co changes the direction of the ordered Pr magnetic moments. While for (Pr,Ho,Tb)Ni_2B_2C single crystals,[24,22,28] the susceptibility data has larger values when the field is applied parallel to the *ab* plane (H∥*ab* plane); for $PrCo_2B_2C$ single crystal, the larger values of susceptibility data in the *c* direction suggest that the alignment of the Pr moments are confined in this direction implying different magnetic structure. However, for deeper insight of the spin sublattice involved, neutron diffraction studies will be necessary to corroborate both, the magnetic transition type and the magnetic structure of this compound.

Figure 3(b) shows the M vs T data at several magnetic fields along the *c* axis. At low magnetic fields, the two magnetic anomalies are clearly seen at 8.5 and 155 K. In order to analyze this behavior, the inset in Fig. 3(b) shows a graph of dM/dT vs T. The intensity of the applied magnetic field influences the magnetic peak at low temperatures. At low field, the peak is at 8.5 K and is shifted to 18 K as the magnetic field is increased. This behavior is similar to that of the $PrNi_2B_2C$ crystal.[22] The effect of the external magnetic field on the anomaly at 155 K is quite different since it tends to

TABLE III. Normal state and superconducting parameters extracted from crystallographic analysis, magnetoresistance, and magnetization measurements. Data in bold belong to this work and is compared with data reported in the literature of homologous Ni-based compounds.

Compound	T_{CO} (K)	ρ_0[a] $\mu\Omega$ cm	RRR	l (Å)	ξ_0 (Å)	dHc_2/dT (kOe/K)	$Hc_2(0)$ (kOe)	$\xi(0)$ (Å)	$\lambda(0)$ (Å)	Ref.
$PrNi_2B_2C$		**3.6**	**10.5**	**97**						**This work**
$PrCo_2B_2C$		**1.7**	**32**	**183**						**This work**
∥ab	**6.0**	**2.4**	**5.5**	**18**	**860**	**−2.986**	**12.003**	**165**	**2722**	**This work**
$PrPt_2B_2C$ **∥c**						**−2.698**	**10.845**	**175**	**2871**	
$LaPt_2B_2C$	10.5	4	5	108	474	−2.700	19.646	110	1650	11
∥*ab*	16.1	1.9	25	190	311	6.23	69.5	69.0	772	27
$LuNi_2B_2C$ ∥*c*						5.51	61.5	73.0	759	
$DyNi_2B_2C$	6.4	2	27	177	778	−1.200	5.322	248		41
∥*ab*	10.5	3.5	18	100	475	−2.00	14.7	150	1160	41
$ErNi_2B_2C$ ∥*c*						−2.60	19.1	131		

[a]ρ_0, residual resistivity; RRR, residual resistivity ratio; l, electron mean free path; ξ_0, BCS coherence length; $Hc_2(0)$, upper critical field; $\xi(0)$, coherence length; $\lambda(0)$, penetration depth.

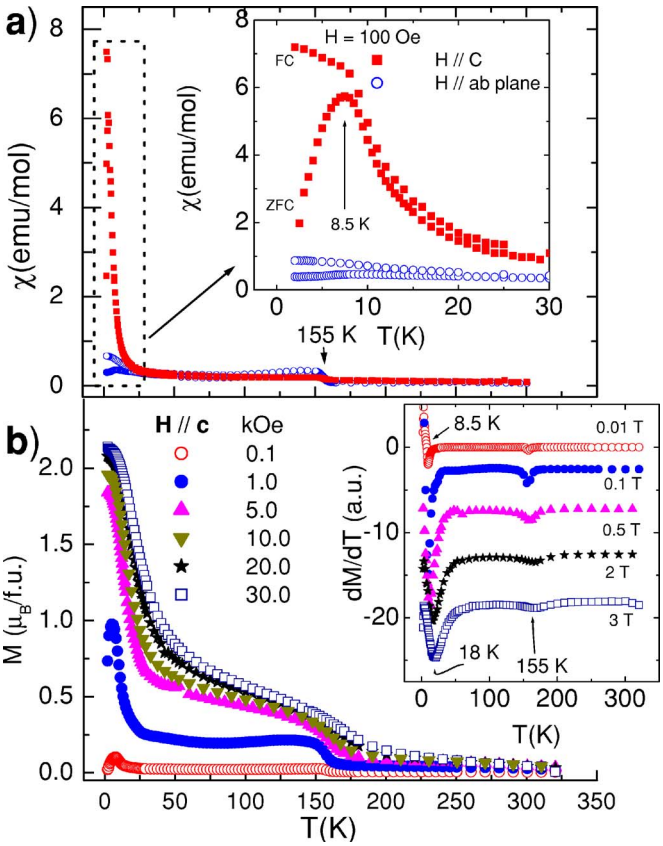

FIG. 3. (Color online) Susceptibility (χ) and magnetization (M) measurements as function of temperature (T) for $PrCo_2B_2C$. Figure 1(a) shows susceptibility data in applied magnetic field of 100 Oe in the *ab*-plane and *c* direction. Inset shows susceptibility details at low temperature in the ZFC and FC modes. Figure 2(b) shows magnetization data measured at different applied magnetic fields in the *c* direction. Inset shows dM/dT as a function of temperature. Arrows indicate the two anomalies at about 8.5 and 155 K.

vanish as the applied field is increased. However, the possibility that this magnetic anomaly arise from another source, such as a small amount of magnetic impurities, is not discarded; literature does not report any combination of quaternary elements giving raise to this type of anomaly at this temperature. For instance, impurities phases such as $PrCo_4B$ ($T_{curie}\sim 459$ K), $PrCo_2B_2$ ($T_{curie}\sim 36$ K), $PrCo_4B_4$ ($T_{curie}\sim 171$ K), $PrCo_{12}B_6$ ($T_{curie}\sim 157$ K), and PrB_2C_2 (van Vleck paramagnet) have not been observed in our samples unless this magnetic signal arise from another unknown Co-B-C phases as was pointed out by Mazumdar *et al.*[29–31] However, as mentioned before, the analysis in the complete diffraction sphere shows no extra spots in the photographic plates. Hence, the possibility that microscopic polycrystalline aggregates were the origin of the secondary magnetic component can be excluded. Accordingly, it can be assumed that the magnetic component is an intrinsic feature of the $PrCo_2B_2C$ phase. To explain such experimental observation it is hypothesized that the occurrence of this magnetic transition arises from the distortion of the tetrahedral TB_4 environment as a result of the short Co-Co bond length and the decrease of the B-Co distance, which is related to the anomalous *ab*-plane

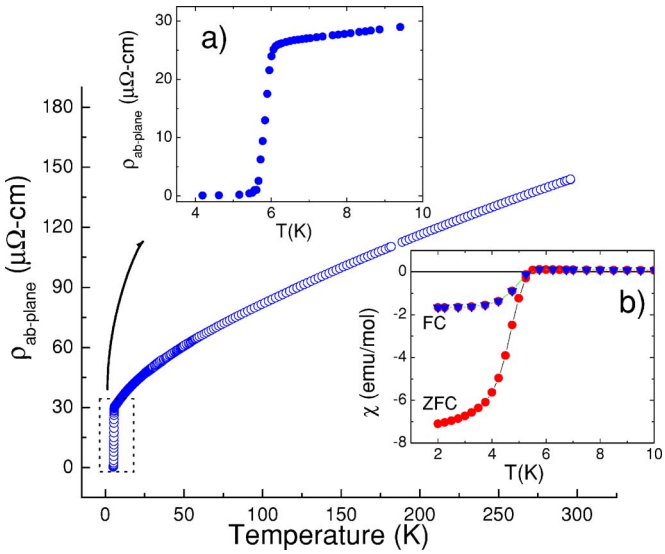

FIG. 4. (Color online) Temperature dependence of the in-plane resistivity from room temperature to 4 K for a $PrPt_2B_2C$ crystal. Inset (a) shows the resistivity at low temperature. Inset (b) shows susceptibility data in the ZFC and FC modes at 10 Oe.

contraction (see Table I). Such distorted structure can alter the antisymmetric exchange in the Co site causing the effect of a weak ferromagnetic order leading to spins canted in the CoB_4 sublattice as has been argued in other borocarbides,[28] although it was generally admitted that the transition metals in the superconducting borocarbide systems are not magnetic. On the other hand, recent studies in Ru/Co-based ruthenocuprates have shown a delicate balance between weak ferromagnetic signal and the change of the Ru/Co environment in the crystalline structure.[32]

C. Magnetoresistance measurements in $PrPt_2B_2C$

Figure 4 shows the in-plane resistivity for $PrPt_2B_2C$ as a function of temperature from 300 to 4 K. The room temperature resistivity is about 144 $\mu\Omega$ cm, whereas the resistivity just above the onset temperature, T_{onset} is 26 $\mu\Omega$ cm. This gives a residual resistivity ratio (RRR) of 5.5, which is higher than the values previously reported in polycrystalline samples ($\sim$1.75).[33] Inset (a) shows the superconducting transition at about 6 K, with a width of 0.35 K, measured between 10% and 90% of the resistivity drop. The ZFC and FC susceptibility measurements corroborate the bulk superconducting state, as seen in the lower right inset (b). A striking feature can be observed in the normal state resistivity as a smooth hump extended over a fairly broad temperature range just above T_c. This feature is not observed in other superconducting materials, we believe that this behavior arises from crystalline electric field effects. Recently, magnetic and heat capacity measurements performed by Dhar *et al.*[33] indicated that the absence of magnetic ordering may be due to splitting of the Pr^{+3} (J=4) ground state as a consequence of CEF, giving raise to a nonmagnetic singlet ground state.

To further explore this anomalous behavior the resistance has been measured without magnetic field, and as a function

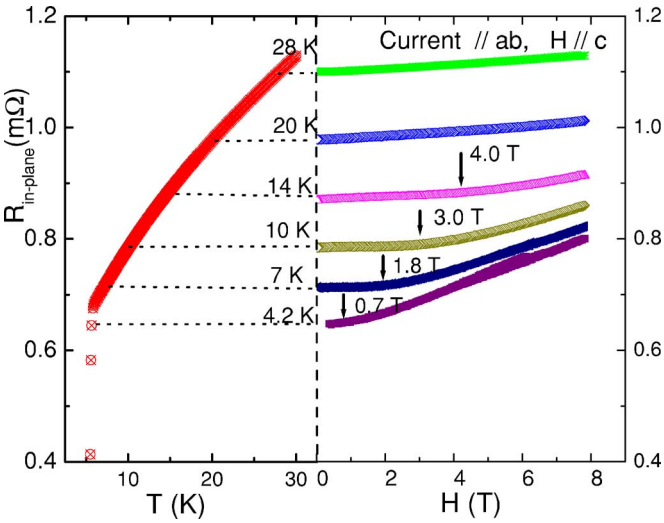

FIG. 5. (Color online) Temperature dependence of the in-plane resistance with no applied field, and resistance-magnetic field at different fixed temperatures between 4.2 and 28 K (horizontal dotted lines) for $PrPt_2B_2C$. The arrows in panel B indicate the applied magnetic field for which a sizable change in the resistance was observed.

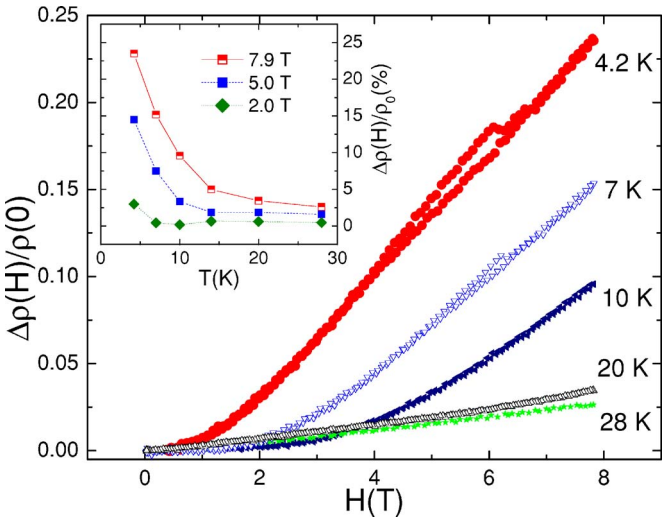

FIG. 6. (Color online) Normalized magnetoresistance, $\Delta\rho(H)/\rho(0)=[\rho(H,T)\text{-}\rho(0,T)]/\rho(0,T)$, for $PrPt_2B_2C$ as function of applied magnetic field at several fixed temperatures. The inset shows the relative magnetoresitance as a function of temperature at 7.9, 5, and 2 Tesla.

of the applied magnetic field for several temperatures. In panel (a) of Fig. 5, the in-plane resistance $R(T)$ is shown from 30 down to 4.2 K without applied magnetic field. Panel (b) shows the transverse magnetoresistance (MR) at different temperatures (28, 20, 14, 10, 7, and 4.2 K) with the applied field parallel to the c axis. There, the real resistance behavior at selected fix temperatures (dotted line) is measured when the applied magnetic field is swept up (H^+) and down (H^-) to 8 Tesla. The results show positive magnetoresistance behavior for all selected temperatures.

Two regions are found in which the resistance does not change when the magnetic field is applied. One region is above 20 K, where no substantial resistance change is evident between $R(H=0)$ and $R(H=7.9\text{ T})$. However, below 14 K a discernible change is observed when the magnetic field is increased. The arrows mark the resistance region where the magnetic field intensity increases the scattering rate, modifying the resistance value. This resistance increase becomes more pronounced at low temperatures. These features can be seen in Fig. 6, where the normalized magnetoresistance, $\Delta\rho(H)/\rho(0)=[\rho(H,T)-\rho(0,T)]/\rho(0,T)$, is plotted at several temperatures. At 28 and 20 K, the $\Delta\rho(H)/\rho(0)$ is small, positive, and proportional to the applied magnetic field, reminiscent of the nonmagnetic analog $(Lu,Y)Ni_2B_2C$ compounds. This behavior was explained by the formation of open orbits at the Fermi surface as were used by Rathanyaka *et al.* and Narozhnyi *et al.*[27,34] to explain the linear behavior and the relative high values of MR in the Lu/YNi_2B_2C compound. They suggest, based on the electronic band structure, that there are open orbits along the c axis which lead to positive and relatively high values of MR; on the contrary, closed orbits at the Fermi surface in this direction could lead to saturation of MR as was observed by Martin *et al.*[35] in polycrystalline copper. In accordance with this behavior, we also speculate that $PrPt_2B_2C$ may present open orbits in this direction and subsequent linear dependence of the MR on the field; however to corroborate this conclusion it will be necessary to perform an electronic band analysis and subsequent MR measurements in the $I\|c$ and $H\|ab$ plane and c configuration. Another remarkable feature in this compound is the magnitude of the MR, which is lower than that obtained for $(Y,Lu)Ni_2B_2C$. This result could be due to the different topology of the Fermi surface with respect to the Y/Lu221 superconducting compounds.

In the inset of Fig. 6, the percent change of the MR as a function of temperature is plotted at three different magnetic fields; 7.9, 5, and 2 T. There is a continuous increase of MR when the temperature decreases, with a maximum at about 25% at 7.9 T and 4.2 K. The MR is positive and varies quadratically with H ($MR\propto H^n$, $n\sim 2$). This behavior is an indication of a typical spin-fluctuation system. The quadratic behavior changes depending on the temperature. For instance, just above T_c (7 K), the quadratic behavior is observed in the overall range of the applied field while at 10 K, MR varies as $n\sim 2.5$ from 0 to 7.9 T. The positive and quadratic behavior of the MR is observed, in general, in systems with AFM ordering,[36] e.g., in the $HoNi_2B_2C$ (T_N=5 K) and HoNiBC (T_N=9.4 K) parent compounds, the MR curves above and below T_N are negative with roughly an H^2 field dependence.[37,38] The negative MR was not expected but it can be attributed to the polarization of the d-band (via RKKY indirect exchange) which induces a small magnetic moment in the Ni layer around this temperature. However, despite the fact that the $PrPt_2B_2C$ in single or polycrystalline form does not present any magnetic order. MR reveals its dependence on the magnetization in the range of studied temperature. This dependence is consistent with the formation of the spin fluctuation, surely from Pt ions since, as already pointed out, it was recently confirmed that the Pr ions in the crystal field split lead to singlet ground state at low temperatures, therefore inducing nonmagnetic

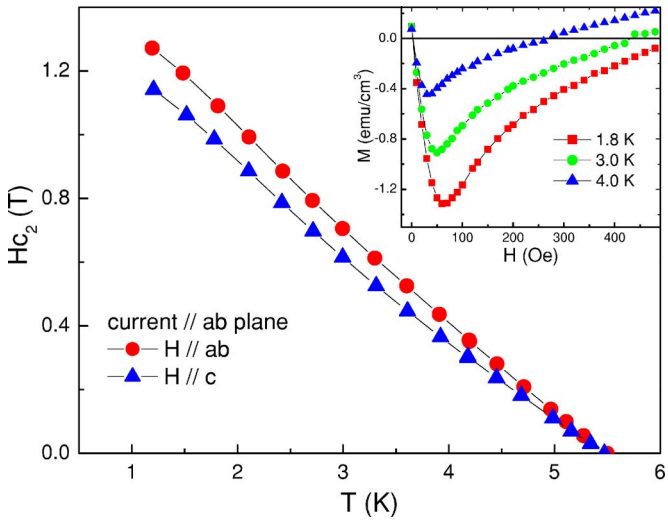

FIG. 7. (Color online) Upper critical field H_{c2} as a function of temperature for the $PrPt_2B_2C$ single crystal under applied fields H parallel to the c axis (open circles) and to the ab plane (filled triangles). There is no sign of saturation down to 1.2 K. The inset shows magnetization as a function of applied field in the H_{c1} regime below T_C.

moment.[33] In this case the positive and quadratic behavior suggests that the $4d$ electrons are not totally quenched, and they are both spatially and temporally correlated playing an important role in the MR behavior and quite likely to the superconducting state.

D. Superconducting characteristics of $PrPt_2B_2C$

Figure 7 presents the plot of the upper critical field (H_{c2}) as a function of temperature from T_c down to 1.2 K. The $H_{c2}(T)$ is almost linear from 5.6 to 2 K in both directions. Below 2 K the data slightly departs from linearity. This fact indicates that neither a magnetic transition, nor intermetallic impurities are present in the Pr/Pt matrix. Furthermore, a small anisotropy was observed with a larger increase of $H_{c2}(T)$ in the ab plane becoming larger at low temperatures. This behavior is very similar to that found in other nonmagnetic borocarbides such as, $LuNi_2B_2C$, YNi_2B_2C.[27] The resulting upper critical field, $H_{c2}(0)$ is about 14.5 and $\sim$13.0 kOe for $H\|ab$ and $H\|c$, respectively. The electronic mean free path was estimated from the formula, $l = 3/2N(0)e^2 v_F \rho_0$, and the BCS coherence length by $\xi_0 = \hbar v_F / T_c$. The experimental value of the residual resistivity was $\rho_0 = 24\ \mu\Omega$ cm, measured just above T_c. The values of $N(0)=4.8$ states/eV cell and $v_F = 3.6\times 10^7$ cm/seg, taken from the band structure calculation for $LuNi_2B_2C$ (Ref. 39) were used. The estimated electronic mean free path was $l \sim 18$ Å, a smaller value than the BCS coherence length, which was estimated to be about $\xi_0 \sim 860$ Å; according to these two values this is a dirty type II superconductor ($\iota \ll \xi_0$). Once this limit is determined, the Ginzburg-Landau (GL) coherence length $\xi(0)$, upper critical field $H_{c2}(0)$, and penetration depth $\lambda(0)$, were extracted from the experimental slope data for each direction (2.986 kOe/K and

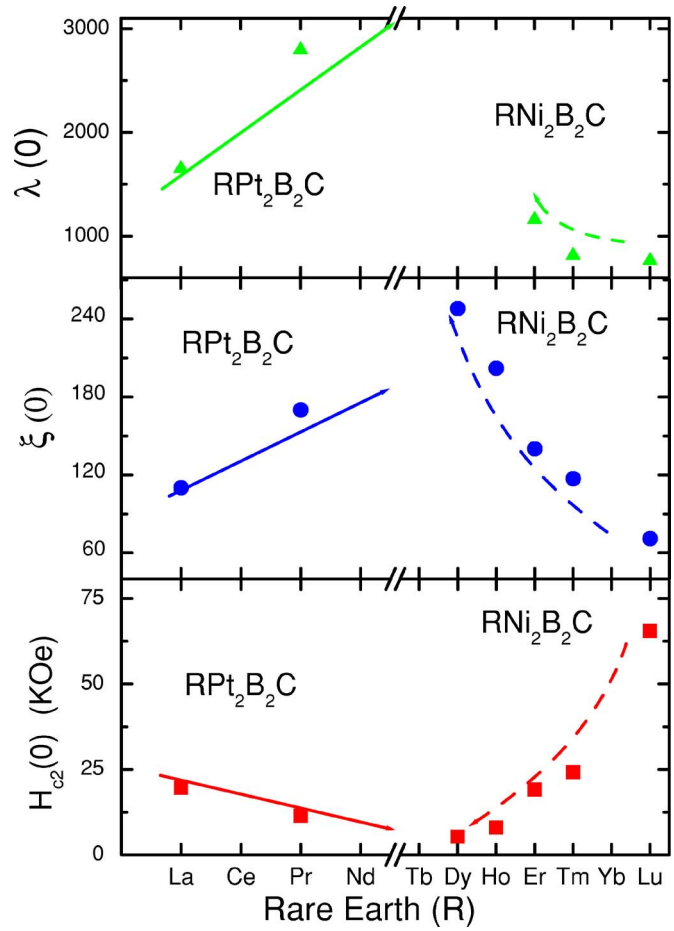

FIG. 8. (Color online) G-L parameters, $H_{c2}(0)$, $\xi(0)$, $\lambda(0)$, for the RPt_2B_2C and RNi_2B_2C series of compounds. Data were extracted from the literature (see text) except for the Pr/Pt compound, which was taken from this work (the solid line and dotted line are guides for the eye).

−2.698 kOe/K for $H\|ab$ and $H\|c$, respectively) in Fig. 7 as well as the value of the lower critical field H_{c1}. In this last case, it was obtained from the isothermal magnetization measurements $M(H)$ at different temperatures; 1.8, 3, and 4 K, in a polycrystalline sample as shown in the inset of Fig. 7. The lower critical field is about 60 Oe at 1.8 K. The Ginzburg-Landau parameter $\kappa(0)$, was determined using $2H_{c1}/H_{c2} = \ln(\kappa) + 0.5/\kappa^2$, and is about 16.5 ± 1. A good agreement was found for the values of $H_{c2}(0)$ and $H_{c1}(0)$ calculated from the G-L relationships: $H_{c2}(0) = 0.693T_c[-dH_{c2}/dT]$ $H_{c1} = (\phi_0/4\pi\lambda^2)(\ln\kappa + 0.5)$, and the experimental extrapolation values $H_{c2}(0)$ and $H_{c1}(0)$ derived from magnetoresistance and magnetization measurements. The values for the $H_{c2}(0)$, $\xi(0)$, and $\lambda(0)$ parameters are listed in Table III and are compared with those values of RNi_2B_2C-related intermetallic compounds. The estimated parameters for $(La,Pr,)Pt_2B_2C$ along with those reported in the literature for RNi_2B_2C are shown in Fig. 8. Both end compounds show the highest T_c and the highest $H_{c2}(0)$. We note that the empty f-electrons belonging to the latter half and the filling earlier half of the rare earth series decrease the T_c and $H_{c2}(0)$ while the Ginzburg-Landau coherence length, $\xi(0)$ and the magnetic

field penetration depth $\lambda(0)$ is increased in $R\mathrm{Pt_2B_2C}$ and $R\mathrm{Ni_2B_2C}$ series. The decrease of H_{c2} and T_c with the rare earth local moment suggests that the superconducting electrons are affected by the R local moment via indirect exchange coupling. The larger decrease of $H_{c2}(0)$ and T_c suggest that superconductivity is strongly affected by the presence of R local moments via indirect exchange coupling. However, at this moment it is difficult to explain the large reduction of these parameters (H_{c2} and T_c) in $\mathrm{PrPt_2B_2C}$ in terms of the picture of the indirect exchange coupling because of the singlet ground state of the $\mathrm{PrPt_2B_2C}$ compound (nonmagnetic). In accordance with this thermodynamic behavior, one could expect superconducting behavior at lower temperatures in the $\mathrm{NdPt_2B_2C}$ compound. Recently, this prediction was confirmed by Paulose *et al.*[40] where a superconducting transition at about 2.8 K was found in this compound.

IV. CONCLUSIONS

We have performed a detailed study of the crystalline structure, magnetization, and magnetotransport properties for $\mathrm{Pr}T_2\mathrm{B_2C}$ (T=Ni, Co, and Pt) single crystals. The structural parameters show an anomalous contraction in the *ab* plane and volume in $\mathrm{PrCo_2B_2C}$, which do not correspond to the ionic radii size and/or chemical pressure effects. Susceptibility data measured in $\mathrm{PrCo_2B_2C}$ show a broad peak at about 8.5 K at low magnetic field, which has been interpreted as an AFM transition. The axis of easy magnetization occurs in the *c* direction instead of along the *ab* plane as seen in the $\mathrm{PrNi_2B_2C}$ compound. The only superconducting system found in this study is the $\mathrm{PrPt_2B_2C}$ crystal with an onset transition temperature at 6 K. Here, the Pt-Pt distance is shorter than in the Pt metallic (fcc structure) suggesting a decrease of the crystal stability for smaller lanthanide ions in the $R\mathrm{Pt_2B_2C}$ series. A positive MR with quadratic field dependence between 4.2 and 7 K is found implying that the 4*d* electrons of Pt ions are not totally quenched. This behavior suggests a spin-fluctuation superconductor system. Finally, the superconducting parameters for the $\mathrm{PrPt_2B_2C}$ compound were determined. The upper critical field, $H_{c2}(T)$, is anisotropic, similar to other nonmagnetic borocarbides. From the values of the electronic mean free path and the coherence length, $\mathrm{PrPt_2B_2C}$ can be classified as a dirty type II superconductor ($\iota \ll \xi_0$) with Ginzburg-Landau parameter $\kappa = 17 \pm 1$.

ACKNOWLEDGMENTS

The authors acknowledge the Centre National de la Recherche Scientifique Max Planck–Laboratoire des Champs Magnetiques Intenses for the time granted to perform the high magnetic field measurements; also F. Morales and A. Briggs for specific heat measurements and discussions. One of the authors (A.D.) thanks the Retención program supported by CoNaCyT. One of the authors (R.F.) thanks PROMEP 20050643 UJATAB-CA175 for support. The authors also thank F. Silvar and J. Palomares for technical help and J. M. Siqueiros for critical reading of this paper.

*Deceased.

[1] E. Tominez, E. Alleno, P. Berger, M. Bhon, C. Mazumdar, and C. Godart, J. Solid State Chem. **154**, 114 (2000); K. H. Muller and V. N. Narozhnyi, Rep. Prog. Phys. **64**, 943 (2001).
[2] L. F. Mattheiss, Phys. Rev. B **49**, 13279 (1994); W. E. Pickett and D. J. Singh, Phys. Rev. Lett. **72**, 3702 (1994).
[3] T. Siegrist, R. J. Cava, J. J. Krajewski, and W. F. Peck, Jr., J. Alloys Compd. **216**, 135 (1994).
[4] J. Ye, T. Shishido, T. Matsumoto, and T. Fukuda, J. Alloys Compd. **275-277**, 76 (1998).
[5] P. Allenspach and U. Gasser, J. Alloys Compd. **311**, 1 (2000).
[6] B. K. Cho, B. N. Harmon, D. C. Johnston, and P. C. Canfield, Phys. Rev. B **53**, 2217 (1996).
[7] B. K. Cho, Physica C **298**, 305 (1998).
[8] B. K. Cho, P. C. Canfield, and D. C. Johnston, Phys. Rev. Lett. **77**, 163 (1996); L. C. Gupta, Physica B **223&224**, 56 (1996).
[9] S. M. Loureiro, C. Kealhofer, C. Felser, and R. J. Cava, Solid State Commun. **119**, 675 (2001).
[10] M. Diviš, K. Schwarz, P. Blaha, G. Hilscher, H. Michor, and S. Khmelevskyi, Phys. Rev. B **62**, 6774 (2000).
[11] R. J. Cava, B. Batlogg, T. Siegrist, J. J. Krajewski, W. F. Peck, Jr., S. Carter, R. J. Felder, H. Takagi, and R. B. van Dover, Phys. Rev. B **49**, 12384 (1994).
[12] V. N. Narozhnyi, J. Freudenberger, G. Fuchs, K. A. Nenkov, D. Eckert, A. Czopnik, and K. A. Müller, J. Low Temp. Phys. **117**, 1599 (1999).
[13] M. El Massalami, H. A. Borges, H. Takeya, R. E. Rapp, and F. A. B. Chaves, J. Magn. Magn. Mater. **279**, 5 (2004).
[14] Y. Y. Xue, P. H. Hor, R. L. Meng, Y. K. Tao, Y. Y. Sun, Z. J. Huang, L. Gao, and C. W. Chu, Physica C **165**, 357 (1990); T. Uzumaki, N. Kamehara, and K. Niwa, Jpn. J. Appl. Phys., Part 2 **30**, L981 (1991).
[15] M. E. López-Morales, D. Rios-Jara, J. Tagüeña, R. Escudero, S. La Placa, A. Bezinge, V. Y. Lee, E. M. Engler, and P. M. Grant, Phys. Rev. B **41**, 6655 (1990); H. A. Blackstead and J. D. Dow, Solid State Commun. **115**, 137 (2000).
[16] O. Peña and M. Sergent, Prog. Solid State Chem. **19**, 165 (1989). Ø. Fisher, A. Treyvaud, R. Chevrel, and M. Sergent, Solid State Commun. **17**, 721 (1975).
[17] E. D. Bauer, N. A. Frederick, P. C. Ho, V. S. Zapf, and M. B. Maple, Phys. Rev. B **65**, 100506(R) (2002).
[18] A. Durán, E. Muñoz, S. Bernès, and R. Escudero, J. Phys.: Condens. Matter **12**, 7595 (2000).
[19] *Siemens*, XSCAnS, Version 2.21 (Siemens Analytical X-ray Instruments Inc., Madison, Wisconsin, 1996).
[20] G. M. Sheldrick, *SHELX97 Users Manual* (University of Göttingen, Germany, 1997).
[21] A. C. Larson, in *Crystallographic Computing*, edited by F. R. Ahmed (Munksgaard, Copenhagen, 1970), pp. 291–294.
[22] A. Durán, S. Bernès, and R. Escudero, Phys. Rev. B **66**, 212510

(2002).
[23] T. Siegrist, H. W. Zandbergen, R. J. Cava, J. J. Krajewski, and W. F. Peck, Jr., Nature (London) **367**, 254 (1994).
[24] J. W. Lynn, S. Skanthakumar, Q. Huang, S. K. Sinha, Z. Hossain, L. C. Gupta, R. Nagarajan, and C. Godart, Phys. Rev. B **55**, 6584 (1997).
[25] C. V. Tomy, G. Balakrishnan, and D. McK. Paul, Physica C **248**, 349 (1995).
[26] M. El Massalami, M. S. da Costa, R. E. Rapp, and F. A. B. Chaves, Phys. Rev. B **62**, 8942 (2000).
[27] K. D. D. Rathnayaka, A. K. Bhatnagar, A. Parasiris, D. G. Naugle, P. C. Canfield, and B. K. Cho, Phys. Rev. B **55**, 8506 (1997).
[28] B. K. Cho, P. C. Canfield, and D. C. Johnston, Phys. Rev. B **53**, 8499 (1996).
[29] C. Chacon and O. Isnard, J. Solid State Chem. **154**, 242 (2000).
[30] H. Onodera, K. Kaneko, T. Onimaru, K. Ohoyama, Y. Yamaguchi, Y. Nemoto, and T. Goto, J. Magn. Magn. Mater. **221**, 293 (2000).
[31] C. Mazumdar, E. Alleno, O. Sologub, P. Salamakha, H. Noel, M. Potel, A. D. Chichure, R. Nagarajan, L. C. Gupta, and C. Godart, J. Alloys Compd. **339**, 18 (2002); M. Mittag, M. Rosenberg, and K. H. J. Buschow, J. Magn. Magn. Mater. **82**, 109 (1989).
[32] R. Escamilla, A. Durán, and R. Escudero, Supercond. Sci. Technol. **18**, 1003 (2005).
[33] S. K. Dhar, A. D. Chinchure, R. Nagarajan, S. M. Pattalwar, L. C. Gupta, E. Alleno, and C. Godart, Phys. Rev. B **65**, 132519 (2002).
[34] V. N. Narozhnyi, J. Freudenberger, V. N. Kochetkov, K. A. Nenkov, G. Fuchs, A. Handstein, and K. H. Müller, Phys. Rev. B **59**, 14762 (1999).
[35] P. M. Martin, J. B. Sampsell, and J. C. Garland, Phys. Rev. B **15**, 5598 (1977).
[36] K. A. McEwen, in *Handbook on the Physics and Chemistry of Rare-Earth*, edited by K. A. Gschneidner, Jr. and L. Eyring (North-Holland, Amsterdam, 1978), Vol. 1, p. 411.
[37] I. R. Fisher, J. R. Cooper, and P. C. Canfield, Phys. Rev. B **56**, 10820 (1997).
[38] M. B. Fontes, J. C. Trochez, B. Giordanengo, S. L. Bud'ko, D. R. Sánchez, E. M. Baggio-Saitovitch, and M. A. Continentino, Phys. Rev. B **60**, 6781 (1999).
[39] W. E. Pickett and D. J. Singh, Phys. Rev. Lett. **72**, 3702 (1994).
[40] P. L Paulose, S. K. Dhar, A. D. Chinchure, E. Allano, C. Godart, L. C. Gupta, and R. Nagarajan, Physica C **399**, 165 (2003).
[41] B. K. Cho, P. C. Canfield, L. L. Miller, D. C. Johnston, W. P. Beyermann, and A. Yatskar, Phys. Rev. B **52**, 3684 (1995); B. K. Cho, P. C. Canfield, and D. C. Johnston, *ibid.* **52**, R3844 (1995).